A New Energy Management Control Method for Energy Storage Systems in Microgrids

Hadis Hajebrahimi, *Student Member, IEEE*, Sajjad Makhdoomi Kaviri, *Student Member, IEEE*, Suzan Eren, *Member, IEEE*, and Alireza Bakhshai, *Senior Member, IEEE*

***Abstract*—This article introduces a new energy management control method for energy storage systems used in dc microgrids. The proposed control method is based on an adaptive droop control algorithm that maintains the dc-bus voltage in the desired range. In the islanded mode of operation, tightly regulating the bus voltage is very challenging. The proposed control technique is based on a nonlinear droop profile with four adaptive parameters. These parameters are determined using the optimization algorithms to achieve reliable and efficient operation. The adaptive parameters enable the proposed nonlinear droop controller to tightly regulate the bus voltage during various changes in loads/sources within a dc MG. The stability of the proposed system for a very wide range of operating conditions is proved. Simulation and experimental results verify the feasibility of the proposed approach and demonstrate its superior performance compared to the conventional controllers.**

***Index Terms*—Adaptive droop control, dc microgrid, energy storage systems (ESSs), renewable energy systems, sequential quadratic programming (SQP) optimization.**

I. Introduction

POWER electronic converters are the main interfaces used in microgrids (MGs) for renewable energy sources (RESs) and energy storage systems (ESSs) [1]. The reliable operation of MGs in hinged on these power electronic converters. In particular, the control system of power converters can make MGs more reliable for future mainstream power generation [2].

Due to the popularity of the ac power system, the development of MG technology has been mostly confined to ac MGs [3], [4]. However, as the number of local MGs increase, the need for long-distance power transmission will significantly decline. In addition, due to the increasing growth of dc loads (e.g., electronic loads, LED lighting systems, electric vehicles, etc.), and increasing utilization of RESs (e.g., solar panels that are inherently dc, and wind turbines that incorporates a dc stage), local dc MGs offer a natural framework for future power systems [5], [6].

In summary, the advantages of the dc MGs over the ac MGs are classified as follows [6], [7]:

Manuscript received May 31, 2019; revised September 27, 2019 and December 29, 2019; accepted February 12, 2020. Date of publication March 5, 2020; date of current version July 20, 2020. Recommended for publication by Associate Editor G. Oriti. *(Corresponding author: Hadis Hajebrahimi.)*

The authors are with the Department of Electrical and Computer Engineering, Queen's University, Kingston, ON K7L3N6, Canada (e-mail: hadis.hajebrahimi@queensu.ca; s.makhdoomi.kaviri@queensu.ca; suzan.eren@queensu.ca; alireza.bakhshai@queensu.ca).

Color versions of one or more of the figures in this article are available online at http://ieeexplore.ieee.org.

Digital Object Identifier 10.1109/TPEL.2020.2978672

1) more efficient operation;
2) reliable operation and less control challenges due to the elimination of reactive power flow and frequency in dc MGs.

Despite the aforementioned advantages of dc MGs, there are various challenges that need to be addressed in order to provide reliable operation of dc-MGs particularly in the islanded mode of operation. In the islanded mode, the MG must be able to provide power balance and supply load currents [8]. Otherwise, the high voltage deviation caused by load changes can be harmful to sensitive loads [9], [10]. Therefore, in islanded dc MGs, one of the critical control tasks is to regulate the common dc-bus voltage [3]–[5], [9]. To achieve this goal, autonomous droop-based control schemes and nonautonomous centralized controllers (that are based on communication links) have been proposed in the literature [10]–[14]. Unlike centralized methods, droop-based methods are not dependent on communication links and have widely been used due to their simplicity and reliability [10]–[12]. However, the existing droop-based techniques cannot offer good performance in terms of reliability, particularly in the islanded mode of operation. In addition, existing droop controllers usually result in very large voltage variations at the dc bus during transients (voltage variations are more significant for smaller systems with low inertia). Large voltage fluctuations are not acceptable for many applications where there are sensitive dc loads connected to the dc bus [3], [4]. In addition, due to a tradeoff between voltage deviation and current sharing, the performance of the conventional droop controllers (i.e., linear constant gain droop) is highly degraded in light load and full load conditions [8]. In particular, to achieve a precise current sharing [i.e., stabilization of constant power loads (CPLs)], high droop gains are preferable, while, in terms of voltage regulation, low droop gains are desirable. Due to the aforementioned tradeoff between current sharing and voltage deviation, conventional droop controllers can not guarantee the optimal performance as well as the tight regulation of MG voltage over a wide range of operating conditions [8]. Fig. 1 shows the tradeoff of the conventional droop control system in a simplified dc MGs with two dc sources. According to Fig. 1, the conventional droop controller with a constant droop gain can not offer a precise and comprehensive solution in both light and full load.

To address the aforementioned drawbacks of the conventional droop controller, different methods have been proposed in the literature [12]–[20]. An energy balancing strategy based on the fuzzy logic algorithm is proposed in [12]. This method incorporates the fuzzy logic algorithms into the droop profile to calculate the virtual resistances of each ESS unit to address

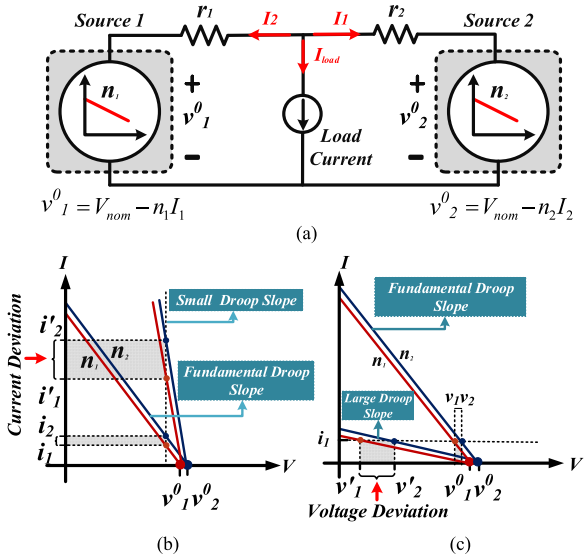

Fig. 1. (a) Simplified dc MG with two DGs. (b) Effect of a small droop gain in the voltage deviation and current sharing error in full load. (c) Effect of a large droop gains in the voltage deviation and current sharing error in light load condition.

the reliability and energy management issues. The prominent drawbacks of this method is the high amount of voltage deviations and circulating currents. An energy management method based on mode-adaptive droop controller is proposed in [13]. Although this method can alleviate the energy management issue, it cannot offer a tight regulation of dc-bus voltage. An adaptive droop control strategy is presented in [14], which provides an accurate load sharing as well as an improved circulating current. According to this method, the interface resistance between the converter terminal and the dc bus should be known in advance or calculated, which is a relatively complex process. A distributed adaptive-droop control with battery energy management capability is presented in [15]. The proposed method is based on a double-layer hierarchical control strategy to simultaneously balance the dc-bus voltage and provide an accurate current sharing between parallel ESSs. Despite the improvements offer by the proposed method, the dependency on communication links limits the application of the proposed controller in practical MGs.

Nonlinear droop control methods are proposed in [16]–[20] to improve the performance of the conventional linear droop controllers. In [17], a control method is proposed to minimize the effect cable resistances, and to improve the voltage regulation and the load sharing compared to linear droop control techniques. According to the presented method, three high-order polynomial droop algorithms are proposed to adaptively adjusts the droop gains. The poor current sharing as well as a highly degraded performance in voltage regulation under heavy-load and light-load conditions are the main drawbacks that limit the application of this method to a narrow range of operating conditions. In [18], a split droop controller is proposed that calculates several different slopes for each load condition to reduce the current sharing and voltage deviation errors. Despite the advantages offered by this method, switching modes created by differences between calculated droop slopes may lead to undesired transients and oscillations inside MG. In [16], [19], and [20], the performance of two nonlinear droop profile (e.g., parabola and programmable droop profiles) are evaluated and compared with the linear droop. According to the presented results, the proposed droop profiles offer an improved performance in both load sharing and voltage regulation. However, both methods demonstrate a poor performance in charging modes of batteries.

In order to address the aforementioned drawbacks of the presented methods, in this article, a novel nonlinear droop controller is proposed, which is able to enhance the dynamic response of the closed-loop control system against transients, tightly regulate the dc-bus voltage, and provide high stability margins against CPLs. The main novelty in the proposed system lies in the hybrid structure of the controller, which incorporates linear dynamics and nonlinear dynamics. This combination can effectively result in a narrower voltage range (i.e., tighter regulations) and provide adaptive damping for the control system, which effectively compensate for the negative impedance caused by CPLs. The proposed control system leads to much faster dynamic response and much more stable operation compared to the state-of-the-art methods.

Unlike the aforementioned nonlinear methods, the presented method offers a precise performance in both negative current (i.e., when battery is in charging mode), and positive current (i.e., when battery is in discharging mode). This lies in the fact that the proposed controller derives droop gains using dc-bus voltage, and state of charge (SOC) of batteries without the need to measure the converter output current. Therefore, this method immunizes the control system from current ripples and sensor errors in comparison to the presented nonlinear methods. In addition, this method is able to change the droop gain smoothly from light load to full load resulting in a smooth droop profile without enforcing switching modes to the control system. According to the presented results and analysis, the voltage deviation and the current sharing are improved in this method in comparison to other nonlinear and conventional droop controllers. This method has been implemented and analyzed in a dc MG operating in islanded mode where the control of the dc-bus voltage is challenging. In order to verify the performance of the proposed controller various power flow scenarios have been analyzed.

The rest of this article is organized as follows. The proposed control system, various operating scenarios, and the definition and ranges of the adaptive parameters are described in Section II. In Section III, the optimal selection of the adaptive parameters is presented. The stability analysis performed in Section IV. Finally, the simulation and experimental results are presented in Section V.

II. Proposed Control System

In order to evaluate the performance of the proposed method, it should be implemented in a practical dc MG. Fig. 2 shows the block diagram of the dc MG implemented in this article. Two ESSs along with two solar energy harvesting systems are connected to the dc bus to feed 4 kW dc loads. According to Fig. 2, the focus of this article is on small-scale dc MGs for residential applications. It is assumed that the line impedances are negligible in comparison with the MG dc load value, which is an acceptable assumption in low-voltage small-scale islanded MGs [14], [20]. Typically, MGs can operate in various operating

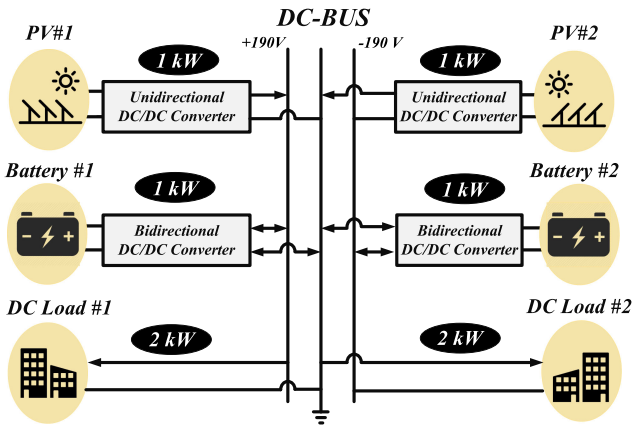

Fig. 2. Implemented dc MG configuration.

modes including islanded and grid-connected modes. In particular, energy devices and systems in which the solar system and battery are connected to the grid/load through power converters have two operating modes as follows.

1) Grid-connected mode: In this mode, the system is connected to the grid and the main task of control the system is to transmit the maximum power to the grid. Therefore, the power converter connected to the solar cells perform maximum power point tracking (MPPT). During this mode, the battery's SOC should be controlled and maintained at a certain level to ensure the availability of enough power for supplying the load in case of transitions to islanded mode. Due to the support of the main grid, the dc-bus voltage is almost constant in this mode.
2) Islanded mode: In this mode of operation, the dc-bus voltage should be regulated within a predefined range (typically 10% of the rated voltage). Without support of the main grid, this task should be done by the power converters connecting distributed sources to the dc bus. In order to ensure efficient extraction of solar energy, the power converter connected to the solar cells perform MPPT. In this case, the main task of the control system of battery converters is to regulate the load voltage by sharing the demanded load power between parallel batteries connected to the dc bus. For instance, if the load voltage decreases (i.e., load demands more power), the battery discharges to inject more power to the dc bus to restore the voltage. On another hand, when the load voltage increases, power should be absorbed by the batteries (i.e., operating in charging mode) to keep the voltage in range. In special cases, when the battery is fully charged/discharged during the islanded mode, the power-sharing and the output voltage regulation can be done by the solar converters. Hence, the solar converter control system evades MPPT and perform power sharing to regulate the dc-bus voltage.

The control system presented in this section guarantee the efficient and reliable operation of dc-MG in islanded mode. In this mode, one of the main drawbacks of the existing droop-based controllers is that the MG components are not utilized in an efficient manner [12], [13], [21], [22]. For instance, in many scenarios, the renewable energy systems have to deviate from their maximum power point to keep the system stable [21], [22].

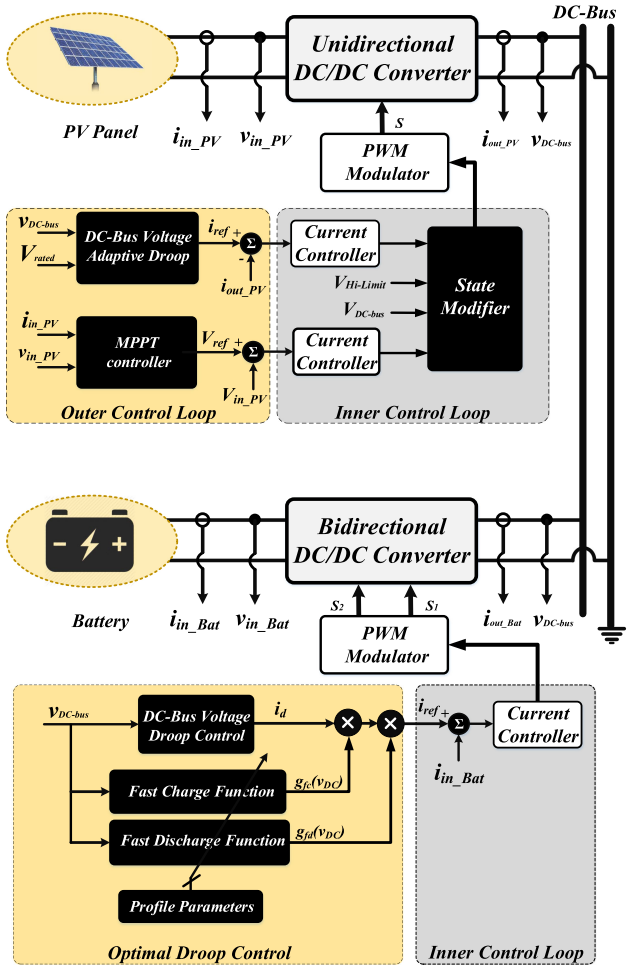

Fig. 3. Block diagram of the proposed control scheme for PV units and ESSs in dc MG.

The main contribution of this article is the fact that the proposed control system allows RESs to operate at their maximum power point whenever it is possible. Fig. 3 shows the general block diagram of the proposed control systems for the solar energy harvesting system and the ESS in dc MG. The proposed control system is effective only during the islanded mode and during the transitions from grid connected to islanded mode and vice versa, different procedures (e.g., island detection, seamless transition, etc.) have to be in place for the reliable operation [23].

According to Fig. 3, the solar control system consists of two cascaded control loops, the inner control loop and the supervisory outer control loop. The inner loop includes the typical PI current controller to control the converter output current [24], and the state modifier block that switches between two control algorithms (i.e., MPPT and the proposed adaptive droop). The state modifier block is given as follows:

$$\begin{cases} \text{if } V_L \le v_{\text{DC}} \le V_H \Rightarrow \text{State} := \text{MPPT Mode} \\ \text{Otherwise} \Rightarrow \text{State} := \text{Droop Mode} \end{cases} \tag{1}$$

where V_L and V_H are, respectively, minimum the maximum allowable dc-bus voltages defined based on the MG requirements and safety standards [25]. This structure provides flexibility to operate at the MPPT as much as possible.

The outer control loop consists of two blocks: the MPPT controller based on perturb and observe algorithm that ensures maximum power is extracted from the solar module [26], and the adaptive dc-bus voltage controller presented in the following.

According to Fig. 3, the ESS control system includes two cascaded control loops as well. The inner control loop includes the PI current controller to control the converter output current, and the supervisory outer loop includes the proposed adaptive droop controller to manage the flow of power between ESS and MG. The rest of this section is dedicated to introducing a novel adaptive droop controller proposed by this article.

The outer loop is an optimized droop controller that incorporates two extra modes (i.e., fast charge and fast discharge) into the control system. These modes are incorporated through two nonlinear functions, $g_{\rm fc}(v)$, $g_{\rm fd}(v)$, presented in the following section ("fc" stands for "fast charge" and "fd" is short for "fast discharge"). These functions effectively determine the speed of charge and discharge of the battery based on the dc-bus voltage. These terms implement a nonlinear adaptive droop profile for the ESS to perform a tighter voltage regulation. Due to the nonlinear nature of the proposed adaptive terms, an optimization algorithm, presented in Section III, is integrated into the control system to determine the optimum nonlinear profiles. Control to systems based on optimization methods can be the proper solutions in determining the critical and unknown parameters of MG systems [27]. In summary, unlike the conventional droop controller, which can only offer two operating modes (charging and discharging), the proposed controller can offer four optimized modes of operation: charging, discharging, fast charging, and fast discharging. Using the two extra modes, the control system is able to offer voltage regulation, while improving the reliability of the system.

According to Fig. 3, the optimal droop controller produces the reference value for the output current of the ESS. Considering the aforementioned description, the adaptive droop profile is given by

$$i_{\rm ref} = i_d(v_{\rm DC}) g_{\rm fc}(v_{\rm DC}) g_{\rm fd}(v_{\rm DC}). \tag{2}$$

According to (2), the generated current reference ($i_{\rm ref}$) includes the linear dc-bus voltage droop term ($i_d(v)$), and the nonlinear fast charge/discharge terms ($g_{\rm fc}(v)$ and $g_{\rm fd}(v)$). Nonlinear terms are presented in the following section. The dc-bus voltage droop term is given by

$$i_d = -k_D \times (V_{\rm nom} - v_{\rm DC}) \tag{3}$$

where k_D, $V_{\rm nom}$, and $v_{\rm DC}$ are the droop coefficient, the nominal dc-bus voltage, and the dc-bus voltage, respectively.

A. Adaptive Parameters Definition

The nonlinear terms $g_{\rm fc}(v)$, $g_{\rm fd}(v)$, presented in (2), are adaptive functions for fast charging/discharging modes. These two functions are given by (when $V_{\rm min} \le v_{\rm DC} \le V_{\rm max}$)

$$g_{\rm fc}(v_{\rm DC}) = \exp\left(\frac{(v_{\rm DC} - V_{\rm fc})}{\alpha_{\rm fc}} u(v_{\rm DC} - V_{\rm fc})\right) \tag{4}$$

$$g_{\rm fd}(v_{\rm DC}) = \exp\left(\frac{(V_{\rm fd} - v_{\rm DC})}{\alpha_{\rm fd}} u(V_{\rm fd} - v_{\rm DC})\right) \tag{5}$$

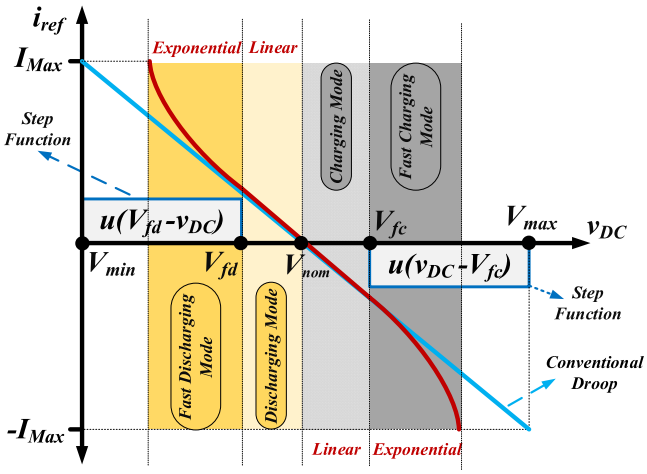

Fig. 4. Performance of the step and exponential functions in the proposed controller.

where $u(x)$ is the unit step function, $\exp(x)$ is the exponential function, $V_{\rm fd}$ and $V_{\rm fc}$ determine the start points for the fast charging and fast discharging modes, respectively, and $\alpha_{\rm fc}$ and $\alpha_{\rm fd}$ are the exponential coefficients for fast charging and fast discharging modes, respectively.

Fig. 4 shows how the current reference is calculated based on the dc-bus voltage for the ESS. According to this figure, the proposed control system provides two extra modes (i.e., fast charge and fast discharge), when the dc-bus voltage is lower than $V_{\rm fd}$ or higher than $V_{\rm fc}$. In particular, when the dc-bus voltage is lower than $V_{\rm fd}$, the load is too heavy and the ESS needs to inject much more power to sustain the dc-bus voltage. On the other hand, when the dc-bus voltage is higher than $V_{\rm fc}$, the generation is higher than the load. Thus, the extra power is used to fast charge the battery.

The main advantages of the profile proposed in Fig. 4 are twofold. It provides a much better dynamical response for the ESS to optimally utilize the available energy. It also limits the range of dc-bus voltage or dc voltage variations. Thus, the converters can operate in a more optimal manner. In addition, the desired voltage deviation range and a precise power-sharing can be achieved autonomously using this method.

The adaptive droop profiles go through the fast charge/discharge modes when the step functions are equal to one. Therefore, the proposed droop profile enables the control system to automatically switch between different operating modes (e.g., fast charge, fast discharge, and linear charge/discharge modes). This feature enables the proposed controller to autonomously absorb/inject more power than the conventional system to prevent the high voltage deviation. Fig. 5 shows the performance of the proposed droop profile in sharing the current and improving the voltage deviation in a dc MG with two similar dc sources. According to Fig. 5, in critical conditions (i.e., when the dc-bus voltage is lower than $V_{\rm fd}$ or higher than $V_{\rm fc}$), the current sharing and voltage deviations are considerably improved in comparison to the conventional droop controller performance shown in Fig. 1.

Fig. 6 shows the flowchart of the control system for ESS. This figure shows the procedure to activate different modes of operation based on the dc-bus voltage. The SOC of the battery

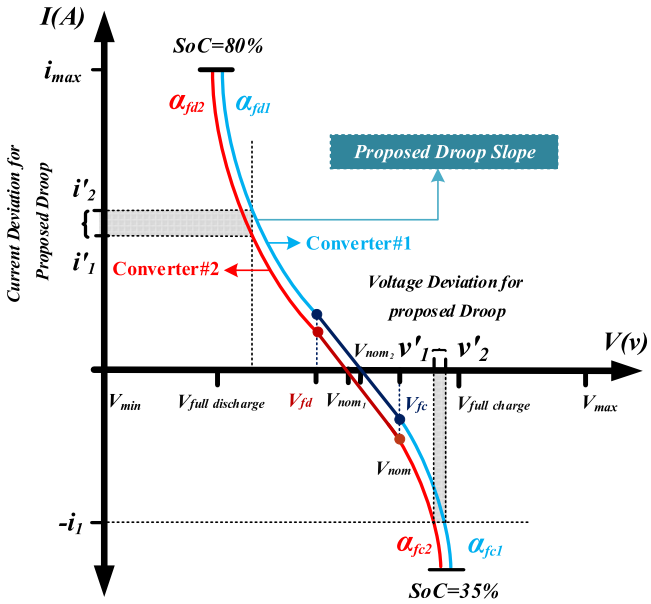

Fig. 5. Performance of the proposed control system for sharing the power between two battery converters, and improving the voltage deviation in a dc MG.

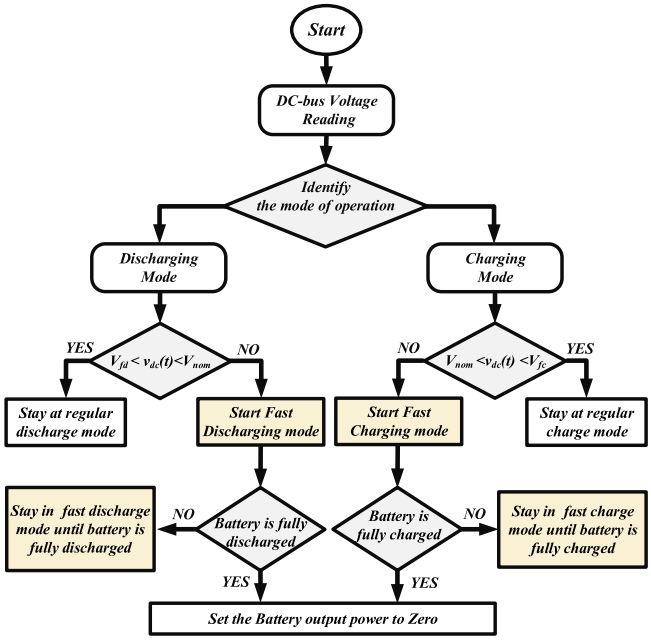

Fig. 6. Flowchart of the proposed control scheme for the ESS.

is a very important factor that has to be considered in selecting different parameters for the proposed profile. Fig. 7 depicts various profiles for different SOC values. This figure shows that the charging and discharging are determined based on the battery conditions in order to sustain the dc-bus voltage.

B. Adaptive Parameters Range

In order to achieve a stable and reliable operation, the numerical domain of functions presented in (2) should be limited. Limitation ranges are defined based on the voltage regulation

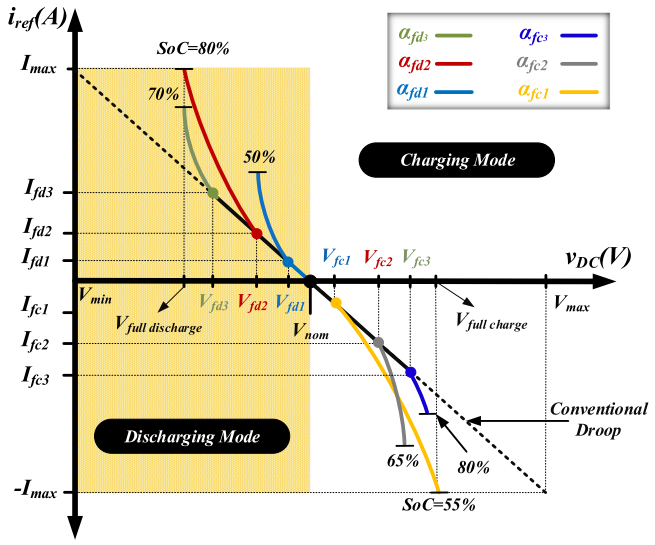

Fig. 7. Proposed adaptive droop controller with adaptive charge/discharge functions.

TABLE I
DC–DC CONVERTER SPECIFICATIONS FOR SIMULATION (S) AND EXPERIMENTAL SETUP (E)

Symbols	Parameters	Values(S)	Values(E)
P_o	Battery#1 converter Output Power	1kW	500W
P_o	Battery#2 converter Output Power	1kW	250W
P_o	PV#1 converter Output Power	1kW	500W
P_o	PV#2 converter Output Power	1kW	0W
f_{sw}	Switching Frequency	100kHz	100kHz
V_{nom}	Nominal DC MG Voltage	190V DC	190V DC
$V_{in_{Bat}}$	Battery Bank Voltage	80V DC	40V DC
$V_{in_{PV}}$	PV Bank Voltage	80V DC	40V DC
L_1	Battery input Inductor	150μH	150μH
L_2	PV input Inductor	330μH	330μH
C_o	Output Capacitor	200μF	200μF

range, the power rating of sources, and the load demanded power. Therefore, the natural Logarithm domain and charge/discharge rate limitations of the implemented batteries are used to specify the values of $\alpha_{\rm fd}$, $\alpha_{\rm fc}$, $V_{\rm fc}$, and $V_{\rm fd}$. According to the simulation of the proposed control system in PSIM software, to ensure the reliable operation of the system in a wide range of operating conditions the lower range of $\alpha_{\rm fd}$ and $\alpha_{\rm fc}$ have to be specified as follows:

$$\alpha_{\rm fc} \geq 2.9 \quad \text{and} \quad \alpha_{\rm fd} \geq 2.9. \tag{6}$$

The parameters listed in Table I are used in this section to define the range of adaptive parameters. The upper range of $\alpha_{\rm fd}$ and $\alpha_{\rm fc}$ are also need to be specified to ensure the reliable operation of the controller. The upper ranges are specified based on the desired range of voltage ($180 \leq v_{\rm DC} \leq 200$) and minimum fluctuations around the rated voltage (1 V in this case). Using the maximum output current of the converter in charging/discharging modes, upper ranges are derived as

$$i_{d_{\rm Max-c}} = -k_D \times (V_{\rm nom} - v_{\rm DC_{max}}) \times g_{\rm fc}(v_{\rm DC_{max}})|_{V_{\rm fc_{min}}} \tag{7}$$

$$i_{d_{\rm Max-d}} = -k_D \times (V_{\rm nom} - v_{\rm DC_{min}}) \times g_{\rm fd}(v_{\rm DC_{min}})|_{V_{\rm fd_{max}}}. \tag{8}$$

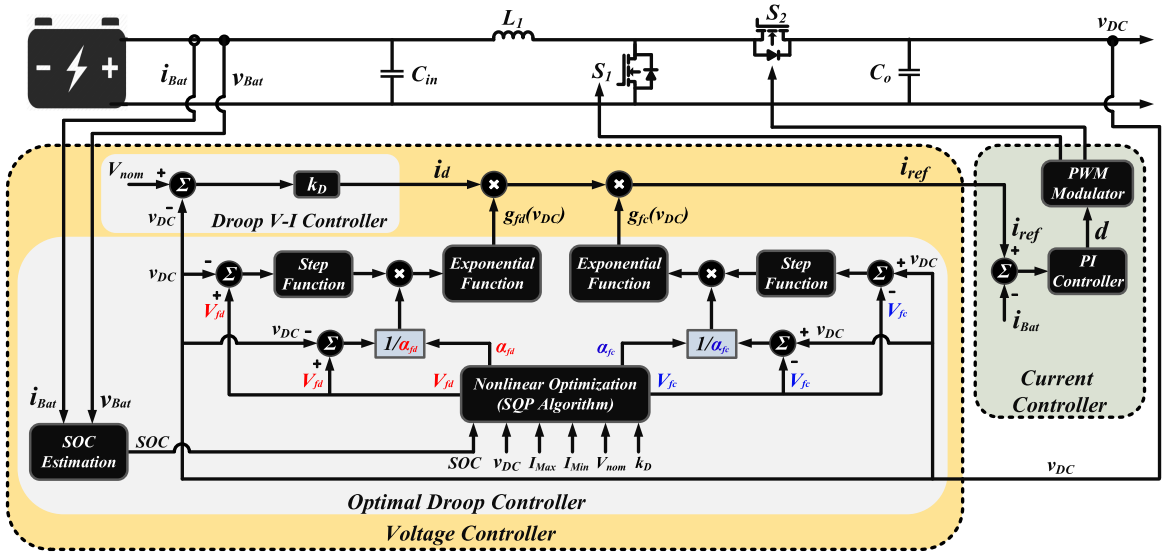

Fig. 8. Detailed block diagram of the proposed control system designed for ESS dc–dc converter.

According to (7) and (8), to ensure the regulation of the voltage in a specific range, the parameters $V_{\mathrm{fc_{min}}}$ and $V_{\mathrm{fd_{max}}}$ need to be specified to keep the desired distance from the rated voltage. In the implemented control system, the proposed range of the dc-bus voltage is considered to be $180 \leq v_{\mathrm{DC-bus}} \leq 200$. Thus, the ranges for the fast charge/discharge voltages are given by

$$V_{\mathrm{fd}} \geq \alpha_{\mathrm{fd_{min}}} \times \mathrm{Min}\left|\ln \frac{i_{\mathrm{ref}} \times \mathrm{SOC}(t)}{(-k_D \times (V_{\mathrm{nom}} - v_{\mathrm{DC}}))}\right| + v_{\mathrm{DC_{min}}} \tag{9}$$

$$V_{\mathrm{fc}} \geq v_{\mathrm{DC_{max}}} - \alpha_{\mathrm{fc_{min}}} \times \mathrm{Max}\left|\ln \frac{-i_{\mathrm{ref}} \times \mathrm{SOC}(t)}{(-k_D \times (V_{\mathrm{nom}} - v_{\mathrm{DC}}))}\right|. \tag{10}$$

Using (6), the upper and lower range of V_{fd} and V_{fc} are given as

$$191 \leq v_{\mathrm{fc}} \leq 198 \quad \text{and} \quad 182 \leq v_{\mathrm{fd}} \leq 189. \tag{11}$$

Finally, by replacing (6) and (11), in (7) and (8), the upper and lower range of α_{fd} and α_{fc} are given as

$$2.9 \leq \alpha_{\mathrm{fc}} \leq 12.8 \quad \text{and} \quad 2.9 \leq \alpha_{\mathrm{fd}} \leq 12.8. \tag{12}$$

Using the derived limits for the proposed control system variables, the reliability and efficiency of the presented method are guaranteed in a wide range of operating conditions.

III. Optimal Droop Control Parameters

In this section, the procedure to determine the optimal values of the parameters for the proposed optimal droop controller is described. The objective is to find appropriate values for four parameters V_{fc}, V_{fd}, α_{fc}, and α_{fd}. The SOC of the battery plays an important role in the calculation of these parameters. The main idea is to devise an optimization algorithm to determine the precise values for the speed and depth of charge/discharge.

The proposed algorithm is based on sequential quadratic programming (SQP) [28], [29], which is an iterative method for nonlinear optimizations. It can handle any degree of nonlinearity, including nonlinearity in the constraints [30]. The suitability of the SQP algorithm to present the optimum solution results is quite straightforward since this gradient search method has already been addressed in the literature as an optimization solution for many real-time applications [31]–[33]. Unlike other presented optimization algorithms based on population heuristics, SQP is based on a profound mathematical theory. SQP algorithm is proven to be one of the most powerful and frequently used algorithms for nonlinearly constrained optimization problems. Its general formulation, the superb numerical performance in terms of accuracy, converge percentage, and efficiency has been validated over the past decades over a wide range of test problems [29]. Fig. 8 shows the detailed block diagram, the proposed control system designed for an ESS dc–dc converter. This diagram shows the nonlinear optimization block with its inputs and outputs. According to this figure, the SQP algorithm calculates the optimal values for the adaptive parameters. The proposed controller uses these values to generate the nonlinear functions $g_{\mathrm{fc}}(v_{\mathrm{DC}})$ and $g_{\mathrm{fd}}(v_{\mathrm{DC}})$. The following steps are implemented in the SQP algorithm.

1) The optimization variables are defined as

$$X = \begin{bmatrix} x_1 \\ x_2 \\ x_3 \\ x_4 \end{bmatrix} = \begin{bmatrix} \Delta V_{\mathrm{fd}} \\ \alpha_{\mathrm{fd}} \\ \Delta V_{\mathrm{fc}} \\ \alpha_{\mathrm{fc}} \end{bmatrix} \tag{13}$$

where $\Delta V_{\mathrm{fd}} = V_{\mathrm{fd}} - V_{\mathrm{nom}}$ and $\Delta V_{\mathrm{fc}} = V_{\mathrm{fc}} - V_{\mathrm{nom}}$.

According to (13), four optimization variables are ΔV_{fd}, ΔV_{fc}, α_{fd}, and α_{fc}. Using the four aforementioned variables, a new optimum operating point can be derived for each value of SOC. To ensure the reliable performance of the control system, three sensitive cases are proposed for system decisions in the optimization process. Two cases occur when the SOC value is high (i.e., higher than 40%) in discharging and charging modes, and another is when the value of SOC is low (i.e., below 40%) in discharging mode. For instance, in discharging mode, when the

value of SOC is higher than 40%, the optimization algorithm is defined to minimize the α_{fd} value while maximizing the value of ΔV_{fd}. This helps the control system to discharge the battery smoothly within a long time with less dc-bus voltage deviation.

2) The general form of the objective function is defined as

$$\text{SQP}: \begin{cases} \text{Minimize } f(X) \\ \text{Subject to}: \begin{cases} H_{\text{eq}}(X) = 0 \\ H_{\text{ineq}}(X) \le 0 \end{cases} \end{cases} \tag{14}$$

where $H_{\text{eq}}(X)$ and $H_{\text{ineq}}(X)$ are the equality and inequality constraints, respectively.

It should be noted that, in the optimization algorithm presented in this article, the $H_{\text{eq}}(X)$ function (i.e., droop profile) is constantly changing by changes of the converter output power. Therefore, the equality constraints are not applicable for this optimization algorithm and two inequality constraints H_{fd}, and H_{fc} are defined to solve the optimization problem. The aforementioned $H_{\text{ineq}}(X)$ functions for charge ($H_{\text{fc}}(X)$), and discharge modes ($H_{\text{fd}}(X)$), are given as follows:

$$\begin{aligned} H_{\text{fd}}(\Delta V_{\text{fd}}, \alpha_{\text{fd}}) &= k_D \times (V_{\text{nom}} - v_{\text{DC}}(t)) \\ &\quad \times e^{u(-v_{\text{DC}}(t)-\Delta V_{\text{fd}}+V_{\text{nom}})\times \frac{(-v_{\text{DC}}(t)-\Delta V_{\text{fd}}+V_{\text{nom}})}{\alpha_{\text{fd}}}} \\ &\quad - I_{\text{max}} \le 0 \end{aligned} \tag{15}$$

$$\begin{aligned} H_{\text{fc}}(\Delta V_{\text{fc}}, \alpha_{\text{fc}}) &= I_{\text{min}} - k_D \times (V_{\text{nom}} - v_{\text{DC}}(t)) \\ &\quad \times e^{u(-v_{\text{DC}}(t)+\Delta V_{\text{fc}}-V_{\text{nom}})\times \frac{(-v_{\text{DC}}(t)+\Delta V_{\text{fc}}-V_{\text{nom}})}{\alpha_{\text{fc}}}} \\ &\quad \le 0. \end{aligned} \tag{16}$$

According to (15) and (16), two optimization functions are required to achieve the optimize performance in both charging and discharging modes. According to (15) and (16), each optimization function includes more than one optimization variable (e.g, α_{fd}, α_{fc}, V_{fc}, and V_{fd}). Therefore, two general cost function are defined to optimize multiple variables simultaneously in both charge and discharge modes. The cost functions for this optimization problem are defined as

1) discharging mode

$$f_1(x) = \Delta V_{\text{fd}} = V_{\text{fd}} - V_{\text{nom}} \tag{17}$$

$$f_2(x) = \alpha_{\text{fd}}. \tag{18}$$

2) charging mode

$$f_1(x) = \Delta V_{\text{fc}} = V_{\text{fc}} - V_{\text{nom}} \tag{19}$$

$$f_2(x) = \alpha_{\text{fc}}. \tag{20}$$

The total cost function is defined as the weighted sum of the aforementioned functions given by

$$f(x) = \sum_{m=1}^{2} w_m f_m(x) = w_1 f_1(x) + w_2 f_2(x) \tag{21}$$

where w_1 and w_2 are the coefficients used to determine the merit of each function in the optimization algorithm.

The SOC of the battery is also incorporated into the optimization algorithm. The multiobjective optimization function is modified to incorporate the SOC

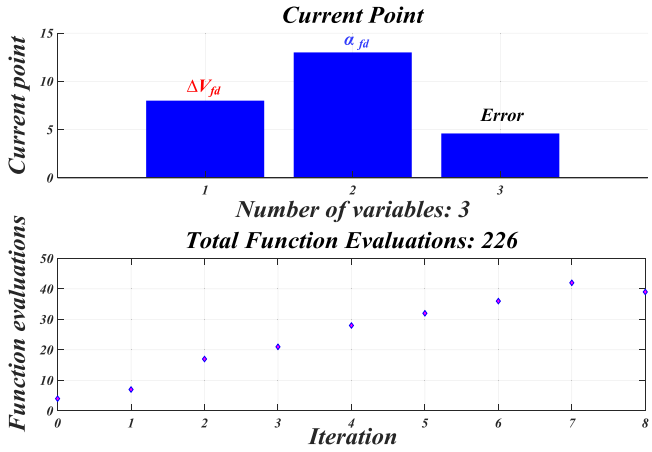

Fig. 9. SQP algorithm performance when SOC = 20%.

1) Case 1

(Discharge mode)

if SOC $\le$ 40%

$$\text{Maximize } f(x) = w_1 \Delta V_{\text{fd}} + w_2 \alpha_{\text{fd}}. \tag{22}$$

2) Case 2

(Discharge mode)

if SOC $\ge$ 40%

$$\text{Minimize } f(x) = w_1 \Delta V_{\text{fd}} - w_2 \alpha_{\text{fd}}. \tag{23}$$

3) Case 3

(Charge mode)

for all SOC values

$$\text{Minimize } f(x) = w_1 \Delta V_{\text{fc}} - w_2 \alpha_{\text{fc}}. \tag{24}$$

According to (22) and (23), two operating cases have been considered for the discharge mode based on SOC values. In case one, the storage system needs to be discharged as slow as possible to prevent storage capacity depletion. This can be done by maximizing $f_1(x)$, and $f_2(x)$. Case 2 simulates the discharging mode when the SOC is more than 40%. In this case, the optimization algorithm tries to maximize $f_2(x)$ while minimizing $f_1(x)$. Equation (24) is defined for the third case where SOC values vary from 20% to 80% in charging mode. According to (24), in charging mode, the control system tends to charge the ESS in a fast-charge rate. It should be noted that for SOC values higher than 80% the special case introduce in Section II is utilizes to regulate the dc-bus voltage. Fig. 9 shows an exemplary optimization case when SOC = 20%. According to Fig. 9, the total function evaluations are 226. In particular, 226 intermediate calculations take place to reach the next optimum solution during eight iterations of running the optimization algorithm. The optimization algorithm continues to run based on an initial error-check that evaluates the objective function before starting any new iteration. Three variables including ΔV_{fc}, α_{fc}, and initial Error are shown in Fig. 9. According to this figure, the optimum calculated values for these variables are 8, 13, and 5,

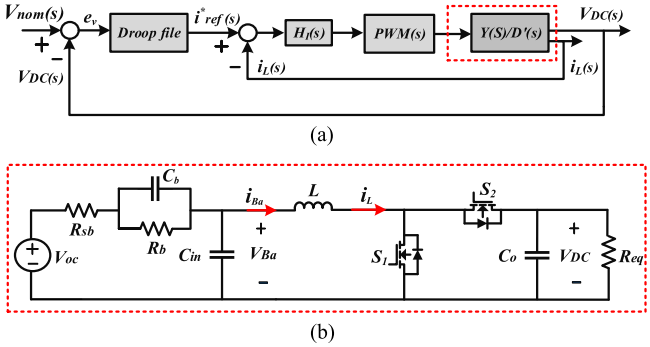

Fig. 10. Block diagram of the ESS closed-loop control system.

respectively, for this specific case. According to the calculated values, when SOC = 20%, the control system performs similar to the conventional droop to discharged the storage system as slow as possible to prevent the depletion of the storage.

IV. Stability Analysis

In this section, the stability analysis of the proposed control method is performed. The proposed optimal droop control system utilizes profiles with linear and nonlinear parts. When the system operates in the linear part (i.e., conventional droop profile), the stability analysis is straight forward. However, nonlinear methods (e.g., the Lyapunov stability theory) must be used to analyze the stability of the nonlinear part (the stability analysis has been carried out only for the islanded mode of operation) [34], [35].

Fig. 10 shows the block diagram of the closed-loop control systems and the schematic diagram of the converter. According to Fig. 10, the dynamical model of the battery is also considered in the schematic block diagram. According to Fig. 10, the state-space model of the ESS is given by

$$\text{State-space}: \begin{cases} \frac{di_L}{dt} = \frac{1}{L}v_{C_{\text{in}}} - \frac{1}{L}v_{\text{DC}} \cdot \acute{d} \\ \frac{dv_{\text{DC}}}{dt} = \frac{1}{C_o} \cdot \acute{d} \cdot i_L - \frac{1}{C_o \cdot R_{\text{eq}}}v_{\text{DC}} \\ \frac{dv_{\text{C}_\text{b}}}{dt} = \frac{V_{\text{oc}} - v_{\text{Cb}} - v_{C_{\text{in}}}}{C_b \cdot R_{\text{sb}}} - \frac{v_{\text{C}_\text{b}}}{C_b \cdot R_b} \\ \frac{dv_{C_{\text{in}}}}{dt} = \frac{V_{\text{oc}} - v_{\text{Cb}} - v_{C_{\text{in}}}}{C_{\text{in}} \cdot R_{\text{sb}}} - \frac{i_L}{C_{\text{in}}} \end{cases} \tag{25}$$

where C_{in}, C_b, C_o, R_{eq}, R_{sb}, and L are the input capacitor of the dc–dc converter, the equivalent series capacitor in the battery model, the dc–dc converter output capacitor of battery, the MG side equivalent load, and the dc–dc converter input inductor, respectively. v_{DC}, $v_{C_{\text{in}}}$, v_{C_b}, i_L, and i_{Ba} are the dc-bus voltage, the input voltage of the dc–dc converter, the voltage across C_b, the inductor current, and the input current of the battery, respectively. Also, $\acute{d} = 1 - d$, where d is duty cycle.

According to (25), the system dynamics include fast changing current, i_L, and slow changing voltages, v_{DC}, $v_{C_{\text{in}}}$, v_{C_b}. Due to different rates of changes, the cascade control system, shown in Fig. 10, includes the fast inner current loop and the slow outer voltage loop. The two loops can be divided into two parts with different rates of change, as the current control loop has much faster dynamics than the comparatively slow voltage control loop. The current control loop is called the fast boundary layer and the voltage loop is named the slow quasi-steady state. In order to analyze the stability of this cascade control loop, the dynamics of the system are separated into the slow dynamics and the fast dynamics.

According to (25) and Fig. 10, the dynamics of the dc–dc converter for the current loop is given by

$$\frac{di_L}{dt} = \frac{1}{L}v_{C_{\text{in}}} - \frac{1}{L}v_{\text{DC}} \cdot \acute{d}. \tag{26}$$

In (26), v_{DC} and $v_{C_{\text{in}}}$ are slow varying relative to the current and considered constants in this equation. In order to design the controller the following Lyapunov function is defined

$$V_i = \frac{1}{2}e_i^2 \tag{27}$$

where $e_i = i_{\text{ref}} - i_L$. By considering (26) and (27), the following controller renders the derivative of the Lyapunov function negative definite

$$\acute{d} = \frac{V_{C\text{in}}}{V_{\text{DC}}} - k_p e_i - k_i \int e_i. \tag{28}$$

According to Fig. 10, the voltage loop includes the nonlinear droop block and the closed-loop block of the inner current control loop. It is worthwhile to mention that the voltage loop does not try to render the voltage error zero. Thus, the asymptotic stability is not required and the boundedness of the voltage variables is the only requirement. In order to investigate the boundedness, the energy function for the voltage error signal is defined as

$$V_v = \frac{1}{2} \times e_v^2 \tag{29}$$

where $e_v = V_{\text{nom}} - v_{\text{DC}}$.

According to (25), the dynamics of the voltage error is given by (due to the fast varying current loop, it is assumed that the inductor current and duty cycle have already reached their final values)

$$\frac{de_v}{dt} = \frac{1}{C_o \cdot R_{\text{eq}}}(V_{\text{nom}} - e_v) - \frac{1}{C_o} \cdot \acute{D} \cdot I_L. \tag{30}$$

The derivative of the energy function (29) is given by

$$\dot{V}_v = \dot{e}_v \times e_v = \frac{1}{C_o \cdot R_{\text{eq}}}\left[(V_{\text{nom}} - \acute{D} \cdot I_L \cdot R_{\text{eq}})e_v - e_v^2\right]. \tag{31}$$

Due to the fact that $(V_{\text{nom}} - \acute{D} \cdot I_L \cdot R_{\text{eq}})$ is close to zero the derivative of the energy function is negative. Thus, the voltage error is bounded.

V. Simulation and Experimental Results

In this section, the simulation and experimental results of the proposed control system are presented. The specifications of the dc–dc converter used in the simulations and the experimental prototype are given in Table I.

The dc MG configuration is shown in Fig. 2 is used to obtain the simulation results. The main concept of the droop-based control methods is based on reducing the voltage deviation created by the variation of the MG load. Therefore, to simulate

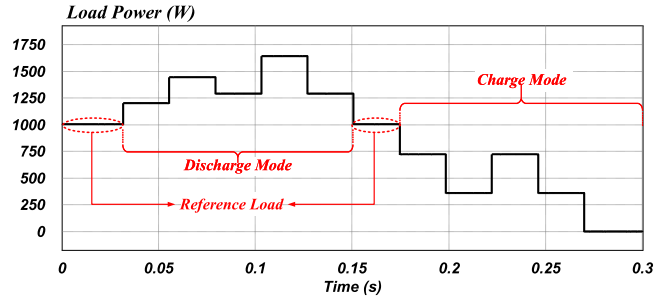

Fig. 11. DC MG load profile (type 1).

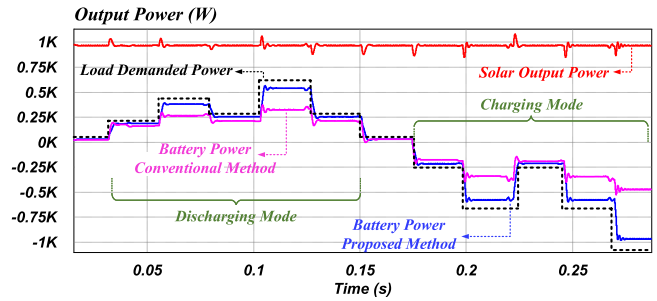

Fig. 12. Transient performance of the proposed control system and the conventional droop controller in changing the battery output power to compensate the load demanded power when SOC = 80%.

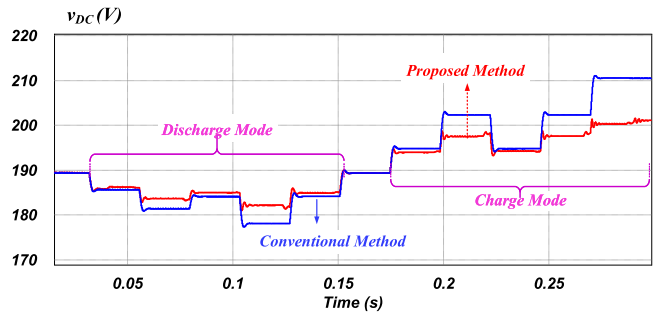

Fig. 13. Transient performance of the proposed control system and the conventional droop controller in regulation of the dc-bus voltage when SOC = 80%.

the voltage deviation, two types of step changes have been applied to the MG load profile. The performance of the proposed control system in the reduction of MG voltage deviation has been compared with the conventional droop method. Fig. 11 shows the first type of load profile implemented to evaluate the control system. The load profile shown in Fig. 11 is utilized in Figs. 12 and 13 to compare the performance of the proposed method with the conventional droop controller in terms of supplying the load demanded power and compensating the load voltage deviations, respectively. According to Figs. 12 and 13, the proposed method can effectively compensate the load demanded power. This leads to significant improvement in the regulation of the dc-bus voltage in comparison with the conventional droop controller. Fig. 13 proves the superior performance of the proposed method in compensating voltage deviations created by the dc load variation in charging and discharging modes.

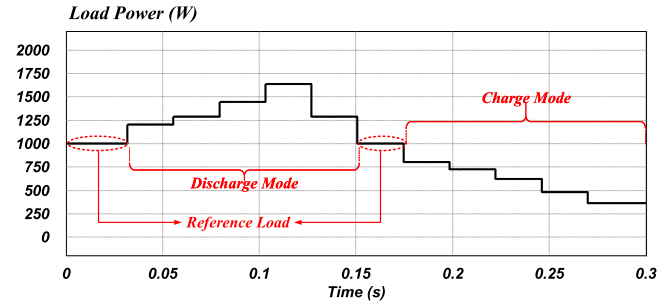

Fig. 14. DC MG load profile (type 2).

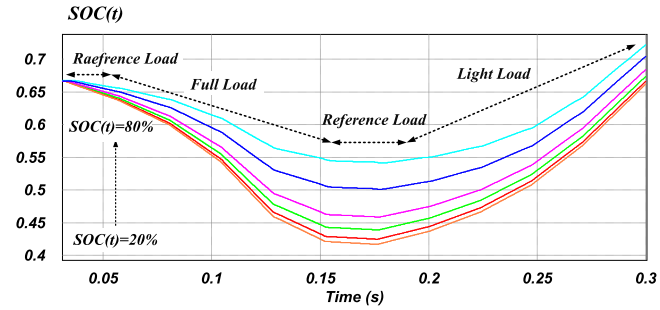

Fig. 15. Battery SOC values when type 2 load is applied to the MG controlled by conventional droop controller.

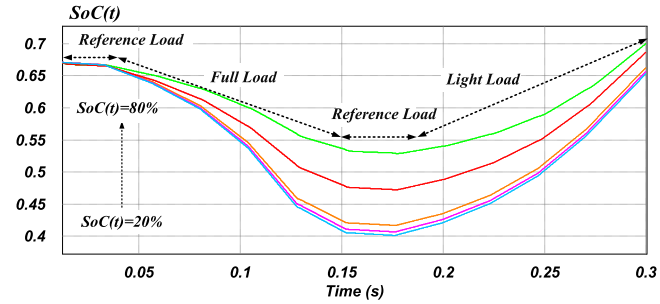

Fig. 16. Battery SOC values when type 2 load is applied to the MG controlled by the proposed controller.

Fig. 14 shows the second type of the dc-load profile implemented to simulate the controller performance in charging/discharging modes. Figs. 15 and 16 shows the profile of the SOC value changes based on the load changes over the simulation time for the conventional and the proposed method, respectively. According to these figures, the proposed control system utilizes the adaptive load profile to supply the demanded load in an efficient manner. For instance, in full load condition in comparison with the conventional droop controller, the proposed controller injected more power to keep the dc-bus voltage in a tight range (i.e., SOC values are lower and more power is injected). These SOC values have been used as the input of the optimization algorithm to obtain the simulation results. According to these figures, each curve belongs to a specific value of the SOC (the SOC values have been varied from 20% to 80% to ensure the optimal operation of the storage systems in a wide range of operation).

Figs. 17 and 18 show the dc-bus voltage variations for different values of SOC for the conventional and the proposed adaptive

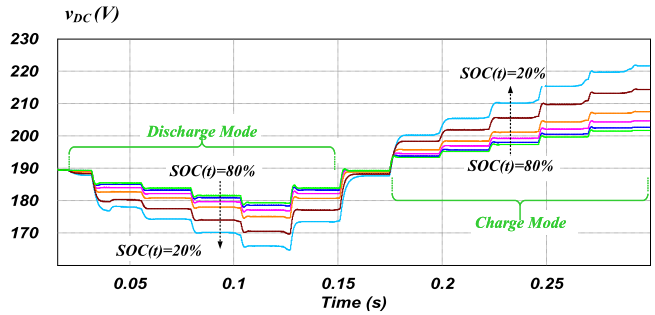

Fig. 17. Transient performance of the conventional droop controller in regulation of the dc-bus voltage in different values of SOC (type 2 load profile).

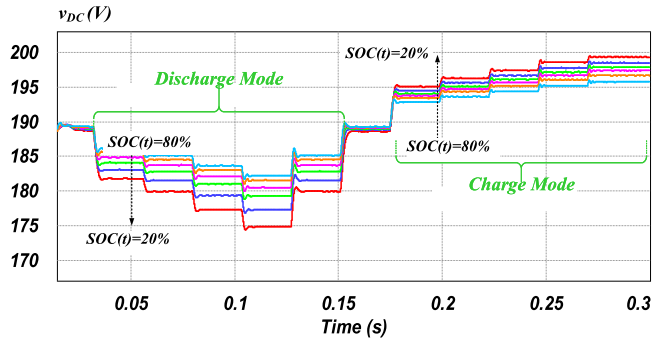

Fig. 18. Transient performance of the proposed controller in regulation of the dc-bus voltage in different values of SOC (type 2 load profile).

droop controllers, respectively. Fig. 18 validates the superior performance of the proposed adaptive droop controller over the conventional one in regulating the dc-bus voltage for a wide range of SOC changes. It should be noted that, in special cases when the voltage is higher than 200 V (i.e., light load condition) and the battery is fully charged (i.e., SOC is higher than 80%), the solar converter control system switches to the droop control mode to keep the dc voltage in the predefined range.

A small-scale dc MG set-up has been implemented to evaluate the performance of the proposed method. The implemented experimental setup includes three boost converters in the power conditioning systems for the two energy storage (battery#1 = 500 W and battery#2 = 250 W) and solar systems (PV panel = 500 W) and a variable dc load. The specifications of the implemented converters are given in Table I. Fig. 19 shows the experimental prototype of the bidirectional dc–dc converters including solar, battery#1, and battery#2 converters. The implemented converters utilized three interleaved phases for optimal implementation (each phase are phase-shifted by 120° to reduce the current ripple). Fig. 20 shows the experimental prototype setup including two battery converters, PV converter, PV simulator, battery simulator, and the variable dc load. The experimental setup has been used to evaluate the proposed control system in practical cases. For cost and safety reasons, the experimental tests are carried out at a reduced power scale $(1/2)$. Experimental results have been obtained based on 200 V nominal voltage with a 40 V voltage variation range (i.e., 10% voltage variation). The SOC values has been varied from 20% to 80%, when the load profile is changing from reference load (500 W) to the light load (50 W) and from reference load to the full-load (1100 W).

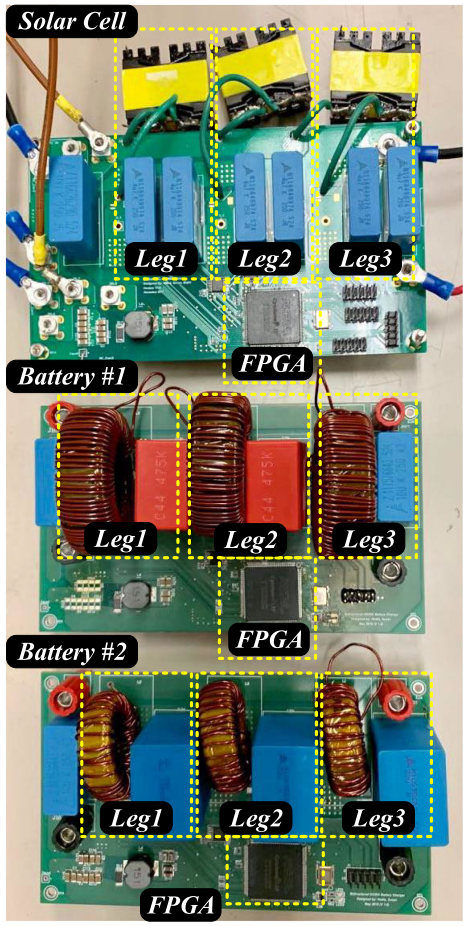

Fig. 19. Prototype dc–dc bidirectional-boost converters including the solar, battery one, and battery two converters.

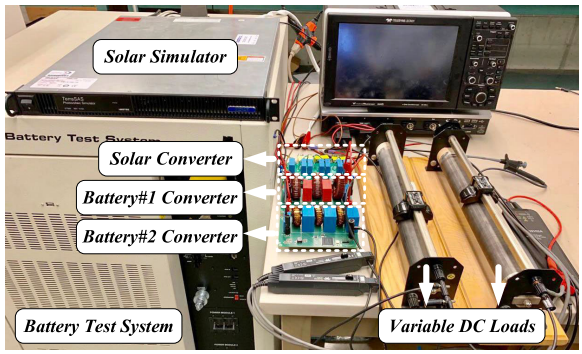

Fig. 20. Experimental setup including two batteries converter, a solar converter, PV simulator, battery test system, and the variable dc load.

In order to evaluate the proposed controller in a wide range of operations, the experimental setup has been tested under light and heavy load conditions with SOC = 40%, SOC = 60%, and SOC = 80%. Table II summarizes the results obtained from the experimental setup. Table II compares the performance of the proposed control system with the conventional droop controller in terms of improving the dc-bus voltage deviation as well as compensating the demanded load power. In order to evaluate the performance of the proposed system over a wide range of load variations in MG, two different cases with different

TABLE II
PERFORMANCE OF THE PROPOSED CONTROL SYSTEM IN IMPROVING THE DC-BUS VOLTAGE DEVIATION AS WELL AS COMPENSATING THE LOAD DEMANDED POWER IN COMPARISON WITH THE CONVENTIONAL DROOP CONTROLLER

Load Step Change	Method	Battery SOC Value	Voltage Deviation	Voltage Deviation Improvement	Compensated Load / Demanded Load		
					Battery #1	Battery #2	Total
Reference to Light Load (500W to 50W)	Conventional	NA (80%)	17V	NA (0%)	0.9A / 1.5A	0.42A / 0.75A	1.32A / 2.25A (58%)
	Proposed	80%	7V	58%	1.2A / 1.5A	0.65A / 0.75A	1.85A / 2.25A (83%)
Reference to Full Load (500W to 1100W)	Conventional	NA (80%)	20V	NA (0%)	1.1A / 2A	0.55A / 1A	1.65A / 3A (55%)
	Proposed	80%	6V	71%	1.8A / 2A	0.93A / 1A	2.73A / 3A (91%)
		60%	11V	45%	1.5A / 2A	0.75A / 1A	2.25A / 3A (75%)
		40%	14V	31%	1.3A / 2A	0.65A / 1A	1.95A / 3A (65%)

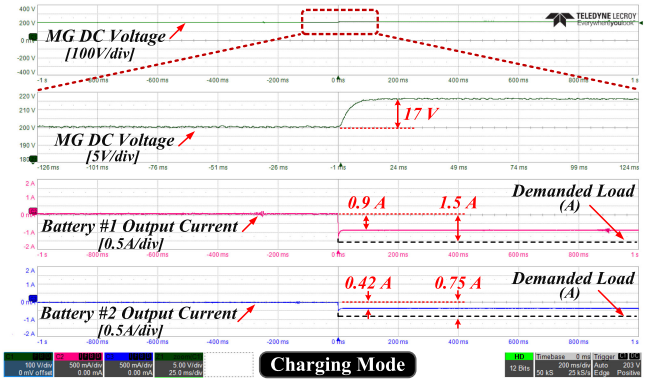

Fig. 21. Transient performance of the conventional droop control system for regulating the dc-bus voltage and sharing the load demanded power between MG converters when the MG load changes from 500 to 50 W and SOC = 80%.

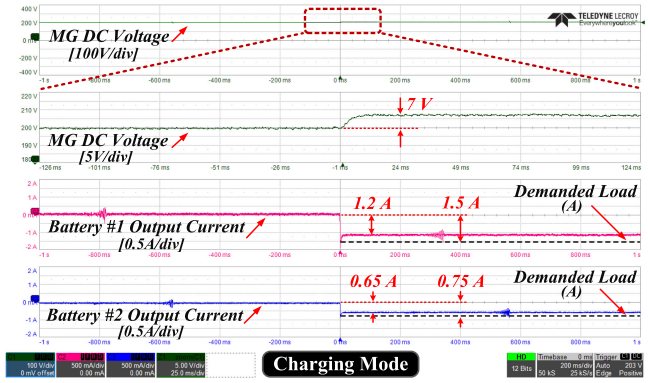

Fig. 22. Transient performance of the proposed control system for regulating the dc-bus voltage and sharing the load demanded power between MG converters when the MG load changes from 500 to 50 W and SOC = 80%.

load profiles are considered Table II. According to Table II, in comparison with the conventional droop, the proposed method offers superior performance over a wide range MG load variation as well as the wide range of available storage capacity (i.e., SOC of batteries). The aforementioned load changing strategies are given as follows.

A. Transition From the Reference Load to the Light Load When the SOC = 80%

Fig. 21 illustrates the performance of the conventional droop control when the load is changing from reference value to the light load (from 500 to 50 W). The maximum voltage deviation in the conventional method is 17 V. Fig. 22 verifies the ability of the proposed controller in maintaining the dc-bus voltage when step changes are applied to the MG load. According to this figure, the proposed controller can successfully regulate the voltage in a tight range (7 V). According to Fig. 22 and Table II, the proposed controller can effectively compensate a higher percentage of load demanded power in comparison with the conventional method while offering a precise current sharing between two battery units.

B. Transition From the Reference Load to the Full Load When the SOC = 80%

Fig. 23 illustrates the performance of the conventional droop control when the load changes from reference value to the full load (from 500 to 1100 W). According to this figure, the maximum voltage deviation in the conventional method is 20 V. Fig. 24 verifies the ability of the proposed controller in maintaining the dc-bus voltage when a step change is applied to the MG load. According to this figure, the proposed controller can successfully regulate the voltage in a tight range (6 V). According to Fig. 24 and Table II, the proposed controller can successfully compensate a higher percentage of load demanded power (i.e., injecting more power to the MG) in comparison with the conventional method while offering a precise current sharing between two battery units.

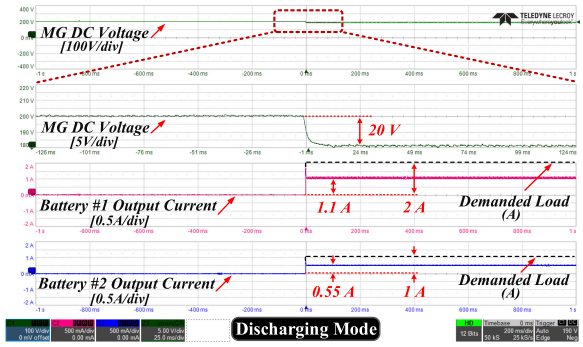

Fig. 23. Transient performance of the conventional droop control system for regulating the dc-bus voltage and sharing the load demanded power between MG converters when the MG load changes from 500 to 1100 W and SOC = 80%.

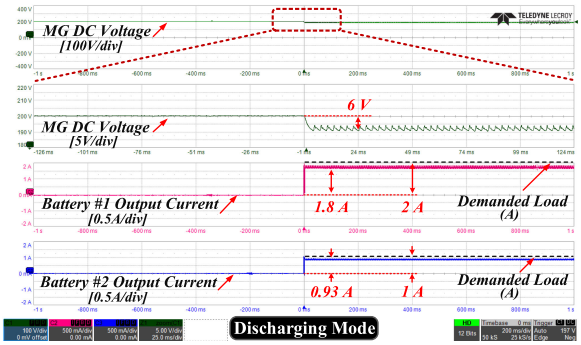

Fig. 24. Transient performance of the proposed control system for regulating the dc-bus voltage and sharing the load demanded power between MG converters when the MG load changes from 500 to 1100 W and SOC = 80%.

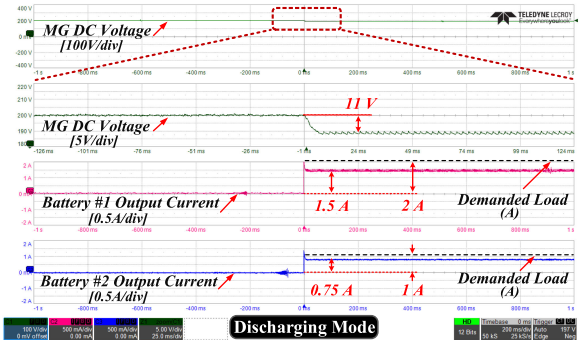

Fig. 25. Transient performance of the proposed control system for regulating the dc-bus voltage and sharing the load demanded power between MG converters when the MG load changes from 500 to 1100 W and SOC = 60%.

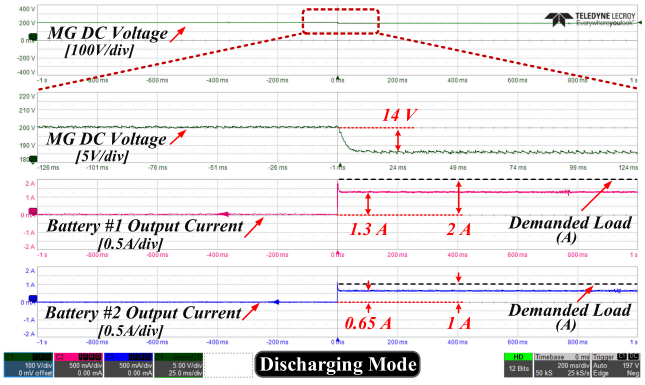

Fig. 26. Transient performance of the proposed control system for regulating the dc-bus voltage and sharing the load demanded power between MG converters when the MG load changes from 500 to 1100 W and SOC = 40%.

C. Transition From the Reference Load to the Full Load When the SOC = 80%, 60%, and 40%

Figs. 24–26 presents the performance of the proposed control system in maintaining the dc voltage at three different values of SOC in discharge mode (e.g, SOC = 80%, SOC = 60%, and SOC = 40%). The voltage deviation in three implemented cases is respectful: 6, 11, and 14 V. According to the results shown in Fig. 26, even in the worst case (SOC = 40%), the proposed control system offers superior performance in comparison with the conventional droop controller. According to Table II, the proposed method offers a precise load sharing among parallel converters for different values of SOCs.

The proposed control system is a supervisory control system that affects the converter controller only in transients. Therefore, it does not impose extra losses and does not affect the efficiency level of the converter.

VI. Conclusion

In this article, a novel adaptive droop control method for the ESS has been proposed for the islanded mode of operation. The proposed technique provides a tight dc-bus voltage regulation, while controlling the charge/discharge of the battery system. In the proposed control scheme, two extra modes (i.e., fast charge and fast discharge) has been introduced, which can offer the optimal performance for the dc MG. Thus, the extra power generated by renewable energy systems can effectively fast charge the batter. In case of voltage drops, the battery is fast discharged, which can maintain the dc-bus voltage. In addition, a nonlinear optimization technique has been used to determine the parameters of the proposed optimal droop controller. Simulation and experimental results have validated the superior performance of the proposed controller in comparison with the conventional ones.

References

[1] F. Blaabjerg, Z. Chen, and S. B. Kjaer, "Power electronics as efficient interface in dispersed power generation systems," *IEEE Trans. Power Electron.*, vol. 19, no. 5, pp. 1184–1194, Sep. 2004.

[2] D. E. Olivares *et al.*, "Trends in microgrid control," *IEEE Trans. Smart Grid*, vol. 5, no. 4, pp. 1905–1919, Jul. 2014.

[3] J. M. Guerrero, J. C. Vasquez, J. Matas, L. G. de Vicuna, and M. Castilla, "Hierarchical control of droop-controlled ac and dc microgrids—A general approach toward standardization," *IEEE Trans. Ind. Electron.*, vol. 58, no. 1, pp. 158–172, Jan. 2011.

[4] J. M. Guerrero, M. Chandorkar, T. Lee, and P. C. Loh, "Advanced control architectures for intelligent microgrids—Part I: Decentralized and hierarchical control," *IEEE Trans. Ind. Electron.*, vol. 60, no. 4, pp. 1254–1262, Apr. 2013.

[5] H. Han, X. Hou, J. Yang, J. Wu, M. Su, and J. M. Guerrero, "Review of power sharing control strategies for islanding operation of ac microgrids," *IEEE Trans. Smart Grid*, vol. 7, no. 1, pp. 200–215, Jan. 2016.

[6] F. Wang, Y. Pei, D. Boroyevich, R. Burgos, and Khai Ngo, "Ac vs. dc distribution for off-shore power delivery," in *Proc. 34th Annu. Conf. IEEE Ind. Electron.*, Nov. 2008, pp. 2113–2118.

[7] J. Park and J. Candelaria, "Fault detection and isolation in low-voltage dc-bus microgrid system," *IEEE Trans. Power Del.*, vol. 28, no. 2, pp. 779–787, Apr. 2013.

[8] Y. Han, H. Li, P. Shen, E. A. A. Coelho, and J. M. Guerrero, "Review of active and reactive power sharing strategies in hierarchical controlled microgrids," *IEEE Trans. Power Electron.*, vol. 32, no. 3, pp. 2427–2451, Mar. 2017.

[9] L. Meng *et al.*, "Review on control of dc microgrids and multiple microgrid clusters," *IEEE J. Emerg. Sel. Topics Power Electron.*, vol. 5, no. 3, pp. 928–948, Sep. 2017.

[10] E. Rodriguez-Diaz, J. C. Vasquez, and J. M. Guerrero, "Intelligent dc homes in future sustainable energy systems: When efficiency and intelligence work together," *IEEE Consum. Electron. Mag.*, vol. 5, no. 1, pp. 74–80, Jan. 2016.

[11] T. Dragičević, X. Lu, J. C. Vasquez, and J. M. Guerrero, "DC microgrids—Part I: A review of control strategies and stabilization techniques," *IEEE Trans. Power Electron.*, vol. 31, no. 7, pp. 4876–4891, Jul. 2016.

[12] N. L. Diaz, T. Dragičević, J. C. Vasquez, and J. M. Guerrero, "Intelligent distributed generation and storage units for dc microgrids—A new concept on cooperative control without communications beyond droop control," *IEEE Trans. Smart Grid*, vol. 5, no. 5, pp. 2476–2485, Sep. 2014.

[13] Y. Gu, X. Xiang, W. Li, and X. He, "Mode-adaptive decentralized control for renewable dc microgrid with enhanced reliability and flexibility," *IEEE Trans. Power Electron.*, vol. 29, no. 9, pp. 5072–5080, Sep. 2014.
[14] S. Augustine, M. K. Mishra, and N. Lakshminarasamma, "Adaptive droop control strategy for load sharing and circulating current minimization in low-voltage standalone dc microgrid," *IEEE Trans. Sustain. Energy*, vol. 6, no. 1, pp. 132–141, Jan. 2015.
[15] T. Dragičević, J. M. Guerrero, J. C. Vasquez, and D. Škrlec, "Supervisory control of an adaptive-droop regulated dc microgrid with battery management capability," *IEEE Trans. Power Electron.*, vol. 29, no. 2, pp. 695–706, Feb. 2014.
[16] F. Chen, R. Burgos, D. Boroyevich, J. C. Vasquez, and J. M. Guerrero, "Investigation of nonlinear droop control in dc power distribution systems: Load sharing, voltage regulation, efficiency, and stability," *IEEE Trans. Power Electron.*, vol. 34, no. 10, pp. 9404–9421, Oct. 2019.
[17] P. Prabhakaran, Y. Goyal, and V. Agarwal, "Novel nonlinear droop control techniques to overcome the load sharing and voltage regulation issues in dc microgrid," *IEEE Trans. Power Electron.*, vol. 33, no. 5, pp. 4477–4487, May 2018.
[18] T. Hailu and J. A. Ferreira, "Piece-wise linear droop control for load sharing in low voltage dc distribution grid," in *Proc. IEEE Southern Power Electron. Conf.*, Dec. 2017, pp. 1–6.
[19] F. Chen, R. Burgos, D. Boroyevich, and W. Zhang, "A nonlinear droop method to improve voltage regulation and load sharing in dc systems," in *Proc. IEEE First Int. Conf. DC Microgrids*, Jun. 2015, pp. 45–50.
[20] T. Dragičević, X. Lu, J. C. Vasquez, and J. M. Guerrero, "DC microgrids—Part II: A review of power architectures, applications, and standardization issues," *IEEE Trans. Power Electron.*, vol. 31, no. 5, pp. 3528–3549, May 2016.
[21] H. Mahmood, D. Michaelson, and J. Jiang, "Decentralized power management of a pv/battery hybrid unit in a droop-controlled islanded microgrid," *IEEE Trans. Power Electron.*, vol. 30, no. 12, pp. 7215–7229, Dec. 2015.
[22] A. Kwasinski, "Quantitative evaluation of dc microgrids availability: Effects of system architecture and converter topology design choices," *IEEE Trans. Power Electron.*, vol. 26, no. 3, pp. 835–851, Mar. 2011.
[23] V. Kleftakis, D. Lagos, C. Papadimitriou, and N. D. Hatziargyriou, "Seamless transition between interconnected and islanded operation of dc microgrids," *IEEE Trans. Smart Grid*, vol. 10, no. 1, pp. 248–256, Jan. 2019.
[24] J. M. Guerrero, J. C. Vasquez, J. Matas, M. Castilla, and L. Garcia de Vicuna, "Control strategy for flexible microgrid based on parallel line-interactive ups systems," *IEEE Trans. Ind. Electron.*, vol. 56, no. 3, pp. 726–736, Mar. 2009.
[25] E. Barklund, N. Pogaku, M. Prodanovic, C. Hernandez-Aramburo, and T. C. Green, "Energy management in autonomous microgrid using stability-constrained droop control of inverters," *IEEE Trans. Power Electron.*, vol. 23, no. 5, pp. 2346–2352, Sep. 2008.
[26] N. Femia, G. Petrone, G. Spagnuolo, and M. Vitelli, "Optimization of perturb and observe maximum power point tracking method," *IEEE Trans. Power Electron.*, vol. 20, no. 4, pp. 963–973, Jul. 2005.
[27] Y. Karimi, H. Oraee, and J. M. Guerrero, "Decentralized method for load sharing and power management in a hybrid single/three-phase-islanded microgrid consisting of hybrid source PV/battery units," *IEEE Trans. Power Electron.*, vol. 32, no. 8, pp. 6135–6144, Aug. 2017.
[28] M. J. D. Powell, "A fast algorithm for nonlinearly constrained optimization calculations," in *Numerical Analysis*, G. A. Watson, Ed. Berlin, Germany: Springer, 1978, pp. 144–157.
[29] P. T. Boggs and J. W. Tolle, "Sequential quadratic programming," *Acta Numerica*, vol. 4, pp. 1–51, 1995.
[30] K. Ritter, "Numerical methods for nonlinear programming problems," in *DGOR/NSOR*, H. Schellhaas, P. van Beek, H. Isermann, R. Schmidt, and M. Zijlstra, Eds. Berlin, Germany: Springer, 1988, pp. 66–85.
[31] M. S. P. Subathra, S. E. Selvan, T. A. A. Victoire, A. H. Christinal, and U. Amato, "A hybrid with cross-entropy method and sequential quadratic programming to solve economic load dispatch problem," *IEEE Syst. J.*, vol. 9, no. 3, pp. 1031–1044, Sep. 2015.
[32] H. Park *et al.*, "Real-time model predictive control for shipboard power management using the IPA-SQP approach," *IEEE Trans. Control Syst. Technol.*, vol. 23, no. 6, pp. 2129–2143, Nov. 2015.
[33] W. Sheng, K. Liu, S. Cheng, X. Meng, and W. Dai, "A trust region SQP method for coordinated voltage control in smart distribution grid," *IEEE Trans. Smart Grid*, vol. 7, no. 1, pp. 381–391, Jan. 2016.
[34] K. Wu, C. W. de Silva, and W. G. Dunford, "Stability analysis of isolated bidirectional dual active full-bridge dc–dc converter with triple phase-shift control," *IEEE Trans. Power Electron.*, vol. 27, no. 4, pp. 2007–2017, Apr. 2012.
[35] R. Wai and L. Shih, "Adaptive fuzzy-neural-network design for voltage tracking control of a dc–dc boost converter," *IEEE Trans. Power Electron.*, vol. 27, no. 4, pp. 2104–2115, Apr. 2012.

Hadis Hajebrahimi (Member, IEEE) received the B.Sc. degree in electrical engineering from the Bahonar University of Kerman, Kerman, Iran, in 2010, and the M.Sc. degree in electrical engineering from Queen's University, Kingston, ON, Canada, in 2018.

She has authored seven journal and conference papers. Her research interests include dc microgrids, smart energy management, and control techniques for power converters.

Ms. Hajebrahimi is a member of IEEE Power and Energy Society.

Sajjad Makhdoomi Kaviri (Member, IEEE) received the M.Sc. degree in electrical engineering from the Isfahan University of Technology, Isfahan, Iran, in 2013, and the Ph.D. degree in electrical engineering from Queen's University, Kingston, ON, Canada, in 2019.

His industrial experience includes collaboration with SPARQ Systems in developing their highly efficient solar microinverter. He has authored 15 journal and conference papers. His research interests include control techniques for dc–dc and ac–dc power converters, microgrids, and smart-grids.

Dr. Kaviri is a member of IEEE Power and Energy Society.

Suzan Eren (Member, IEEE) received the B.Sc. degree (first class honors), the M.Sc. and Ph.D. degrees in electrical engineering from Queen's University in 2006, 2008, and 2013, respectively.

She is currently an Assistant Professor with the Electronics and Communication Engineering Department, Queen's University, Kingston, ON, Canada. She has authored 48 peer-reviewed papers and holds 11 U.S. patents. Her research interests include the control and design of power converters used in microgrids and renewable energy systems.

Dr. Eren is a member of ePOWER, the Queen's Center for Energy, and Power Electronics Research. She has received several academic scholarships, including the 2011–2012 Bert Wasmund Scholarship for Sustainable Energy Research. She has extensive academic and industrial experience developing highly efficient power converters. She is the recipient of both the 2017–2018 and 2018–2019 Professor of the Year Award by the second year electrical engineering student body. She is the current IEEE Kingston Section Chair.

Alireza Bakhshai (Senior Member, IEEE) received the B.Sc. and M.Sc. degrees from the Isfahan University of Technology, Isfahan, Iran, in 1984 and 1986, respectively, and the Ph.D. degree from Concordia University, Montreal, QC, Canada, in 1997.

He is currently a Professor with the Department of Electrical and Computer Engineering, Queen's University, Kingston, ON, Canada. From 1998 to 2004, he served on the faculty of Electrical and Computer Engineering, Isfahan University of Technology. He has acquired 38 international patents (11 granted and 17 pending) patents, and published more than 50 peer-reviewed journal and more than 100 conference papers in fields including high-power electronics and applications, renewable energy conversion, and control systems.

Dr. Bakhshai is a licensed Professional Engineer in Ontario.